

Soil production on a retreating escarpment in southeastern Australia

Arjun M. Heimsath* Department of Earth Sciences, Dartmouth College, Hanover, New Hampshire 03755, USA
 John Chappell Research School of Earth Sciences, Australian National University, Canberra ACT 0200, Australia
 William E. Dietrich Department of Geology and Geophysics, University of California, Berkeley, California 94720, USA
 Kunihiro Nishiizumi Space Sciences Laboratory, University of California, Berkeley, California 94720, USA
 Robert C. Finkel Center for Accelerator Mass Spectrometry, Lawrence Livermore National Laboratory, Livermore, California 9455, USA

ABSTRACT

The functional dependence of bedrock conversion to soil on the overlying soil depth (the soil production function) has been widely recognized as essential to understanding landscape evolution, but was quantified only recently. Here we report soil production rates for the first time at the base of a retreating escarpment, on the soil-mantled hilly slopes in the upper Bega Valley, southeastern Australia. Concentrations of ^{10}Be and ^{26}Al in bedrock from the base of the soil column show that soil production rates decline exponentially with increasing soil depth. These data define a soil production function with a maximum soil production rate of 53 m/m.y. under no soil mantle and a minimum of 7 m/m.y. under 100 cm of soil, thus constraining landscape evolution rates subsequent to escarpment retreat. The form of this function is supported by an inverse linear relationship between topographic curvature and soil depth that also suggests that simple creep does not adequately characterize the hillslope processes. Spatial variation of soil production shows a landscape out of dynamic equilibrium, possibly in response to the propagation of the escarpment through the field area within the past few million years. In addition, we present a method that tests the assumption of locally constant soil depth and lowering rates using concentrations of ^{10}Be and ^{26}Al on the surfaces of emergent tors.

Keywords: erosion, cosmogenic nuclides, landscape evolution, geomorphology, tors.

INTRODUCTION

Rates of bedrock conversion to soil were recently shown to decline with increasing local soil thickness on a hilly landscape in northern California, thus defining empirically the soil production function (Heimsath et al., 1997, 1999). However, the dependence of soil production on soil depth has not been measured extensively. Here we examine a soil-mantled landscape at the base of a passive margin escarpment in the Bega Valley, southeastern Australia, to quantify the relationship between soil production and depth. We also use concentrations of ^{10}Be and ^{26}Al from the surfaces of emergent bedrock outcrops, or tors, to test whether soil thickness has remained constant while the ground surface has been lowering.

Recent modeling studies have suggested that the pace of escarpment retreat on passive margins depends on the rate of conversion of bedrock to erodable material (e.g., Kooi and Beaumont, 1994; Tucker and Slingerland, 1994; van der Beek and Braun, 1999). Maximum rates of soil production, occurring where soil is thinnest or absent (Heimsath et al., 1997), set the limiting lowering rates for soil mantled landscapes. This study constrains the retreat rates and sediment transport processes of an erosional escarpment, thus furthering our understanding of a largely unsolved problem for tectonic geomorphology.

THEORY

Soil production in coastal California was determined from soil depth-topographic curvature relationships and cosmogenic nuclides (Heimsath et al., 1997, 1999). The first method rests on a simple mass balance, neglecting mass loss in solution, between the change in mass of the soil column and the balance between soil produced from the underlying bedrock and the divergence of the sediment transport flux, \tilde{q}_s (Fig. 1A),

$$\rho_s \frac{\partial h}{\partial t} = -\rho_r \frac{\partial z_b}{\partial t} - \nabla \cdot \tilde{q}_s, \quad (1)$$

where h is soil thickness, z_b is the elevation of the soil-bedrock boundary, ρ_s and ρ_r are the bulk densities of soil and rock, respectively, and t is time. Heimsath et al. (1997, 1999) assumed linear soil creep ($\tilde{q}_s = -\rho_s K \nabla z$) and also assumed steady-state local soil depth ($\partial h/\partial t = 0$), to show

$$\varepsilon(h) = -\frac{\rho_s}{\rho_r} K \nabla^2 z, \quad (2)$$

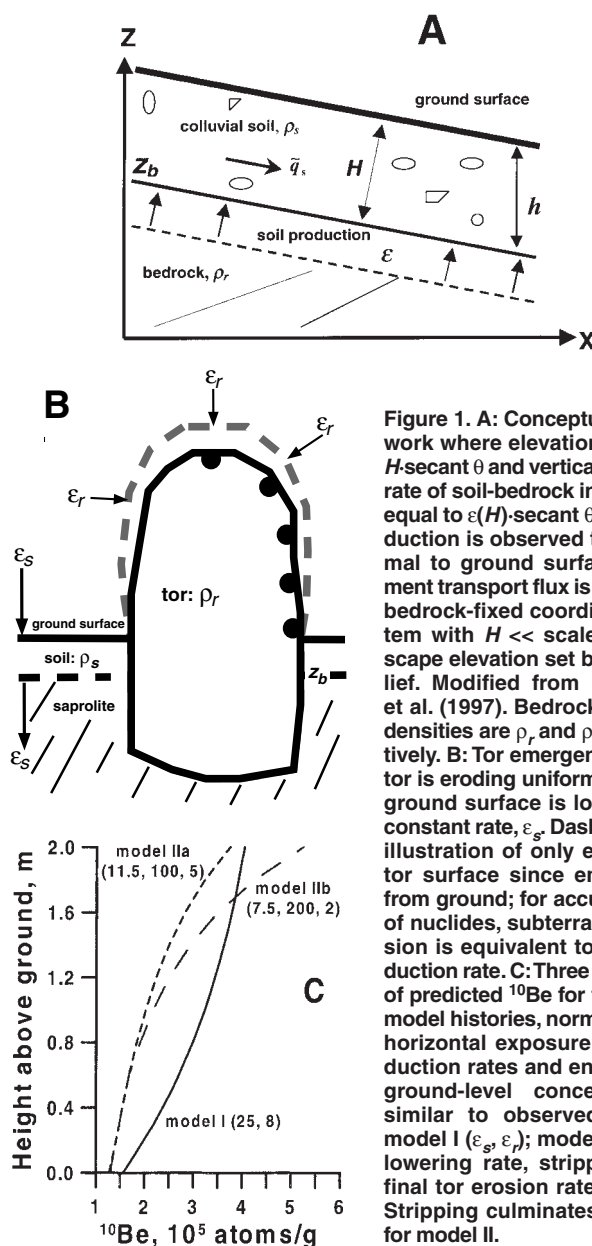


Figure 1. A: Conceptual framework where elevation, $z = z_b + H$ -secant θ and vertical lowering rate of soil-bedrock interface is equal to $\varepsilon(H)$ -secant θ . Soil production is observed to be normal to ground surface. Sediment transport flux is \tilde{q}_s . This is bedrock-fixed coordinate system with $H \ll$ scale of landscape elevation set by total relief. Modified from Heimsath et al. (1997). Bedrock and soil densities are ρ_r and ρ_s , respectively. **B:** Tor emergence where tor is eroding uniformly, ε_r , and ground surface is lowering at constant rate, ε_s . Dashed line is illustration of only erosion of tor surface since emergence from ground; for accumulation of nuclides, subterranean erosion is equivalent to soil production rate. **C:** Three examples of predicted ^{10}Be for tor profile model histories, normalized for horizontal exposure and production rates and ending with ground-level concentrations similar to observed values: model I ($\varepsilon_s, \varepsilon_r$); model II (initial lowering rate, stripping rate, final tor erosion rate, m/m.y.). Stripping culminates at 20 ka for model II.

*E-mail: arjun.heimsath@dartmouth.edu.

where K is a diffusion coefficient with dimensions L^2T^{-1} , z is the ground surface elevation, and $\epsilon(h)$ is the soil production rate. This formula neglects the difference between vertical and slope-normal soil depth, H (Fig. 1A). Equation 2 led Heimsath et al. (1997) to regard topographic curvature as a proxy for soil production. Measurements of soil depth and slope curvature in northern California indicated that soil production declined exponentially with normal depth,

$$\epsilon(H) = \epsilon_0 e^{(-\alpha H)}, \quad (3)$$

where ϵ_0 is the production rate with zero soil cover ($m \cdot m \cdot yr^{-1}$), and α is a rate constant. Without a known diffusivity, K , however, the rates cannot be quantified.

Soil production also can be evaluated using cosmogenic nuclides, produced by cosmic ray interaction with common nuclei in rock and soil minerals. The concentration, C , of a nuclide depends on its production rate, which depends on depth, z_x , and its radioactive decay (e.g., Lal, 1991),

$$\frac{dC}{dt} = P_0 e^{-\mu z_x} - \lambda C, \quad (4)$$

where P_0 is the nuclide production rate at a flat surface, μ is the absorption coefficient (material density divided by the mean attenuation length for cosmic rays, $\Lambda \sim 165 \pm 10 \text{ g cm}^{-2}$), and λ is the nuclide decay constant ($\lambda =$

$\ln 2/t_{1/2}$, where $t_{1/2} = 1.5 \times 10^6 \text{ yr}$ for ^{10}Be and $t_{1/2} = 7.01 \times 10^5 \text{ yr}$ for ^{26}Al). Under steady state, when $t \gg (\lambda + \mu\epsilon)^{-1}$ with constant erosion and constant soil depth, the nuclide concentration is

$$C = C_0 e^{-\lambda t} + P(H, \theta) \left(\frac{1}{\lambda + \mu\epsilon_s} \right), \quad (5)$$

where $P(H, \theta)$ is the nuclide production rate ($\text{atom g}^{-1}\text{yr}^{-1}$) at the soil-bedrock boundary on a slope, θ , and C_0 is the initial concentration of the nuclide (Lal, 1991). $P(H, \theta)$ is calculated as a factor of surface production: 6 (^{10}Be) and 36.8 (^{26}Al) atoms $\text{g}^{-1}\text{yr}^{-1}$ for sea level and high latitude ($>60^\circ$) (Nishiizumi et al., 1989; Lal, 1991; Dunne et al., 1999). Under steady state, the soil production rate equals the erosion rate and is determined from measured ^{10}Be and ^{26}Al , with C_0 assumed to be zero.

Equation 5 depends on a local steady-state assumption. Here we propose an independent test of this, based on emergent tors. Tors are corestones from within the weathering zone that emerge as the surrounding saprolite is eroded; the concentrations of nuclides on the tor surfaces thus depend on the subsurface exhumation history as well as the subaerial, bare-rock erosion rate, ϵ_r .

We consider two patterns of tor exposure history: (I) a steady-state model with constant soil thickness and constant soil production and tor erosion rates (Fig. 1B); and (II) a model where steady-state erosion is followed by an episode of accelerated erosion (stripping) leading to tor emergence, after which the tor surface erodes at a rate ϵ_r . We integrated equation 4 numerically using standard Runge-Kutta methods to determine nuclide concentrations on a tor surface for both models instead of using Lal's (1991) steady-state solution. The program was checked with the constant erosion case and replicated exactly results from Lal's solution. As shown in Figure 1C, the profile of predicted nuclide concentrations under steady-state (model I) conditions is quite different from model II profiles.

STUDY AREA

Nunnock River is a tributary to the Bega River that descends from steep granitic slopes of the eastern Australian escarpment and drains into the Pacific Ocean, through Late Silurian to Early Devonian granite and granodiorite of the Bega batholith (Lewis and Glen, 1995) (Fig. 2). The high-relief, steep-faced escarpment, which probably has retreated inland from a rift-initiated margin (Ollier, 1982; Seidl et al., 1996; Weissel and Seidl, 1997), separates a highland region of gentle topography, low relief, and slow erosion rates (e.g., Young, 1983; Bishop, 1985; Wellman, 1987; Nott, 1992) from a coastal belt with higher denudation rates (O'Sullivan et al., 1996). Relief is about 200 m between the study area and the coast and increases to the escarpment, which rises to about 950 m and is covered with intermediate to wet sclerophyll forest with patches of dense understory in the valley bottoms. Rain falls throughout the year, $\sim 910 \text{ mm yr}^{-1}$ (Bureau of Meteorology, Australia, 1999). The southeastern highlands above about 700 m were affected episodically by periglacial processes in the Pleistocene (e.g., Galloway, 1965; Caine and Jennings, 1968; Costin, 1972) and sediment transport processes and rates may have fluctuated (e.g., Butler, 1967). These effects appear to have been negligible at our low-elevation site, where there is no evidence for the episodic sedimentation and denudation (e.g., Butler, 1967; Prosser et al., 1994). The absence of texture contrast or stratified soils further supports this, but we test it explicitly with our tor model.

Soil production and transport appeared to be primarily due to biogenic processes, although there was some evidence of overland flow. Burrowing wombats (*Vombatus ursinus*) were the most obvious agents of soil disturbance and their burrows, $\sim 30 \text{ cm}$, occur widely across the landscape. Burrowing echidnas (*Tachyglossus aculeatus*), scraping lyre birds (*Menura novatehollandiae*), and worms are also important in southeastern Australia (Paton et al., 1995). Tree throw also uproots bedrock and distributes sediment, but at our site such features were shallow and there was little evidence of pit-mound topography. A well-defined, thin ($<1 \text{ m}$) soil mantled the underlying saprolite and bedrock. Soils showed no horizonation beyond a thin

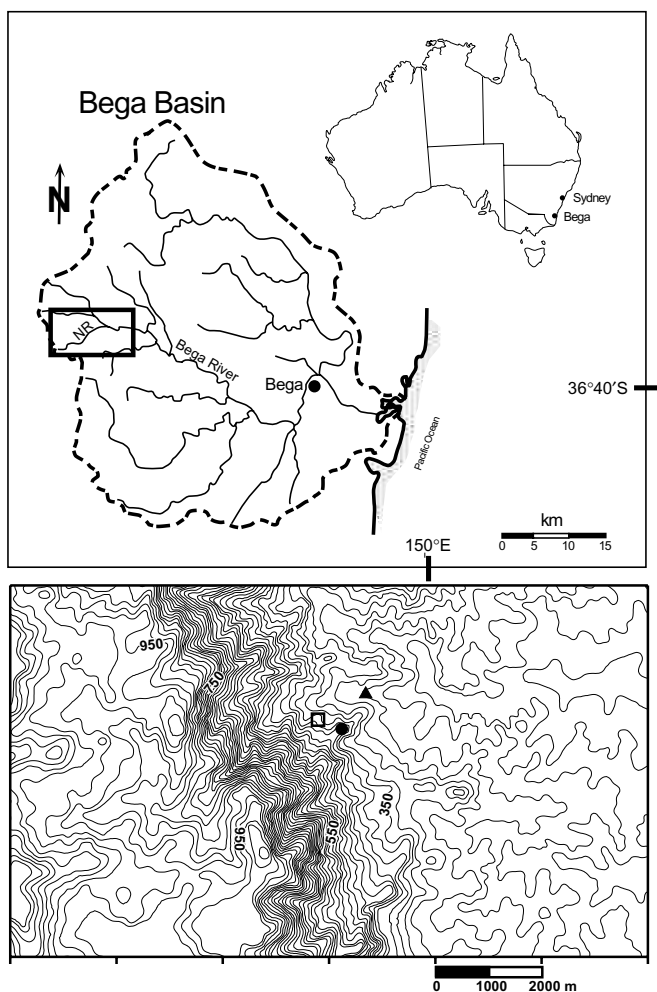


Figure 2. Location map showing close proximity with escarpment at head of Bega basin. Topography of inset rectangle is with 20 m contour intervals from 1:100 000 digital data (Australian Surveying and Land Information Group) from Bega (sheet 8824) map. Black dot on ridge crest shows tor locations; open square shows surveyed area; and black triangle shows stream sediment site.

TABLE 1. SOIL PRODUCTION RATES FROM COSMOGENIC NUCLIDE CONCENTRATIONS

Sample	Depth* (cm)	Slope	H-slope factor#	Elev. (m)	Wt (g)	Be (mg)	Al (mg)	¹⁰ Be atoms/g quartz (sea level)	+/- ²⁶ Al	+/- ²⁶ Al / ¹⁰ Be	E (m/m.y.)	+/- E	Age (k.y.)			
NR1	90	17	0.30	389	50.64	0.457	6.08	513300	13560	3059000	123700	5.96	0.71	9.25	1.10	86.81
NR2	10	12	0.87	395	52.26	0.442	6.52	113700	3048	624100	44060	5.49	0.53	45.60	4.43	18.02
NR3	12	15	0.85	388	50.16	0.459	6.70	107100	4036	601500	28560	5.62	0.48	47.87	4.12	17.16
NR4	60	17	0.45	386	50.80	0.459	6.60	249100	6337	1353000	63090	5.43	0.55	20.61	2.08	39.58
NR5	42	16	0.58	378	50.37	0.458	6.33	168300	5067	1080000	55570	6.42	0.61	28.24	2.67	28.94
NR6	30	12	0.68	404	50.04	0.462	6.81	148000	4590	829300	71830	5.60	0.64	34.51	3.95	23.74
NR7	28	9	0.72	404	52.10	0.450	6.63	195700	5981	1087000	50750	5.55	0.48	26.08	2.27	31.34
NR9	40	15	0.64	385	52.53	0.458	7.21	234600	6083	1402000	108300	5.97	0.65	20.82	2.27	39.22
NR10	47	24	0.50	377	53.65	0.460	7.43	262900	6572	1503000	76230	5.72	0.54	18.97	1.80	42.86
NR11	22	23	0.71	383	51.18	0.461	6.40	87590	2627	522300	38550	5.96	0.61	56.53	5.78	14.53
NR12	0	0	1.00	381	42.63	0.458	4.83	60130	2461	342800	47670	5.70	0.90	68.04	10.70	9.68
NR13	52	20	0.49	389	50.78	0.460	5.91	319000	8122	1870000	86310	5.86	0.56	15.26	1.45	53.23
NR14	15	14	0.82	399	50.40	0.460	6.41	166500	3714	1012000	47550	6.08	0.49	29.45	2.39	27.80
NR15	66	21	0.39	389	50.61	0.463	6.58	229900	6233	1308000	72660	5.69	0.62	21.83	2.38	37.32
NR22	Riv.	0	1.00	412	50.73	0.462	6.14	79390	2574	451400	28060	5.69	0.53	51.49	4.75	12.77
NR23	40	15	0.64	420	55.27	0.404	7.21	152800	8297	931600	63630	6.10	0.69	25.62	2.90	25.55

Cosmogenic nuclide concentrations and apparent erosion rates from tor samples**

NR16	0	0	1.00	420	49.39	0.404	5.85	176300	9584	1040000	38670	5.90	0.53	21.69	1.94	28.91
NR17	110	80	0.58	420	52.91	0.404	6.76	332200	10560	2072000	91200	6.24	0.51	10.94	0.89	56.87
NR18	160	0	1.00	420	52.80	0.405	7.23	392000	12590	2277000	66390	5.81	0.43	9.56	0.71	64.92
NR19	20	75	0.62	420	48.85	0.404	6.14	161000	8213	1024000	49840	6.36	0.59	22.83	2.12	27.53
NR20	140	75	0.62	420	52.55	0.407	6.80	370900	14320	2239000	114000	6.04	0.54	9.95	0.88	62.52
NR21	250	0	1.00	420	48.03	0.407	6.87	398400	10900	2472000	74040	6.20	0.49	9.07	0.71	68.29
NR8	10	10	1.00	394	37.74	0.458	3.70	153100	4063	881600	53210	5.76	0.52	26.29	2.35	24.89

Note: All errors are propagated to the soil production or erosion rate, E, and ²⁶Al and ¹⁰Be concentrations are normalized to sea-level, high-latitude production rates of 36.8 and 6 atoms g⁻¹ yr⁻¹ (Lal, 1991; Nishiizumi et al., 1989).

*The average soil density is 1.2 g/cm³ and the site location is lat 36.62 degrees S, long 149.5 degrees E.

#The H-slope factor corrects for soil depth and slope shielding for all samples (Dunne et al., 1999).

**Samples are from the sides and top of one tor (2.5 m), top of an adjacent one (1.6 m), and top of an emergent tor (0 m).

(<15 cm), organic-rich A horizon and a relatively homogeneous B horizon. Tors protruded on nearby ridge crests, and erode by grain-by-grain spallation and by thin (1–2 cm) exfoliation sheets.

RESULTS

Soil production rates determined from ²⁶Al and ¹⁰Be concentrations in 14 bedrock or saprolite samples from the soil-bedrock interface are in Table 1. Figure 3 plots the soil production rates, calculated with equation 5, against observed soil depth. A variance-weighted best-fit regression defines the following soil production function,

$$\epsilon(H) = (53 \pm 3) \cdot e^{-(0.020 \pm 0.001)H}, \tag{6}$$

where the soil production rate is in meters per million years and the soil depth is in centimeters. Scatter around the regression line shown in Figure 3 is small and is significantly less than for the California data of Heimsath et al. (1997). Analytical uncertainties from the relatively clean granitic quartz were small and the soil-bedrock boundary was clearly defined. The lack of scatter also suggests that no episodes of major disturbance occurred during the time required to generate the soil (i.e., 20–100 k.y.) and that bio-

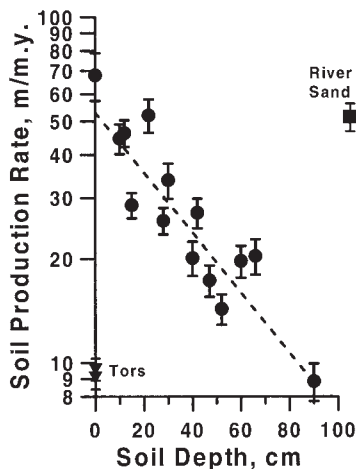


Figure 3. Soil production function (see text equation 6). Solid black circles are averages of rates from both ¹⁰Be and ²⁶Al (Table 1), and error bars represent all errors propagated through nuclide calculations, i.e., uncertainty in atomic absorption, accelerator mass spectrometry, bulk density and soil depth measurements, and attenuation length of cosmic rays. Black triangles are erosion rates from two highest tor samples, NR-21 and NR-18 (Table 1).

turbation, highly variable in space and introducing scatter, may have less effect on the soil production depth dependence here than at the California sites. A catchment average erosion rate of 51.5 ± 4.8 m m.y.⁻¹, determined from a stream sediment sample, is plotted to the right of the soil depth axis.

We measured ¹⁰Be and ²⁶Al concentrations from seven samples from two tors (Table 1). Results plotted against height above ground level match well a theoretical concentration profile, calculated for steady-state conditions, with $\epsilon_s = 25$ m m.y.⁻¹ and $\epsilon_r = 8$ m m.y.⁻¹ (Fig. 4). The observed profile shows increasing nuclide concentrations with height above ground, leading to apparently decreasing erosion rates, where 9 m m.y.⁻¹ from the top sample is least likely to show any legacy. Similarly, the best-fit value for ϵ_s fits well the soil production rate of 26 m m.y.⁻¹ obtained by equation 6 for observed soil depths around the tors of 35 cm. The good fit of the observed with the theoretical profile supports the steady-state lowering assumption.

The soil production function compares closely with nuclide-based results from California, but the soil depth curvature data highlight a complexity in process. A plot of topographic curvature versus soil depth shows a well-defined linear relationship (Fig. 5). There is no relationship between soil depth and slope, nor do the modest slopes (<25°) suggest nonlinear sediment transport processes. For the divergent areas of the site the soil production function, equation 6, can be substituted for $\epsilon(h)$ in equation 2, using the data in Figure 5

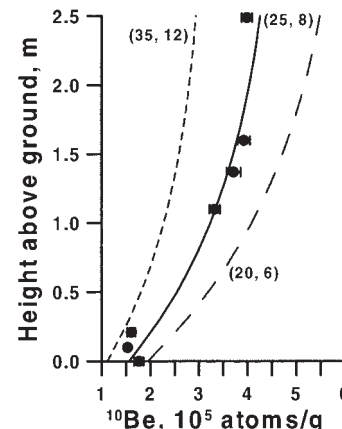


Figure 4. Predicted and observed concentrations of ¹⁰Be for tor profile (²⁶Al results are equivalent). ¹⁰Be is plotted with height above present ground surface, with measured nuclide concentrations normalized to sea level (Table 1) and error bars as in Figure 3. Black line plots best-fit model prediction. Dashed lines from ϵ_s , ϵ_r (respectively) suggest, with Figure 1C, that best fit is not unique solution.

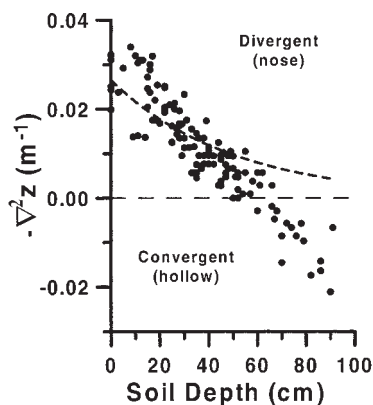


Figure 5. Negative curvature, $-\nabla^2 z$, versus normal soil depth times cosine of local slope. Curvature calculated as in Heimsath et al. (1999) with 5 m grid. Short-dashed line is not fit to data, but shows expected exponential relationship when equation 6 is set equal to equation 2, indicating predicted relationship under linear creep transport only.

to solve for the K that yields the best-fit overlay of the curvature and nuclide data. The bulk density ratio between rock and soil was 2.0, and solving for K yielded $40 \text{ cm}^2 \text{ yr}^{-1}$. This is similar to the average K for 34 sites in California, Oregon, and Washington: $49 \pm 37 \text{ cm}^2 \text{ yr}^{-1}$ (McKean et al., 1993).

DISCUSSION AND CONCLUSIONS

The nuclide-based soil production function reported here supports the form of equation 3, as defined by Heimsath et al. (1997). Furthermore, the spatial variation of soil production rates suggests a landscape out of morphologic equilibrium, similar to northern California. Here this disequilibrium may be in response to the propagation of the escarpment through the field area. Other studies determined slow rates of erosion ($\sim 10 \text{ m m.y.}^{-1}$) for the southeastern highlands, west of the escarpment (e.g., Wellman and McDougall, 1974; Young, 1983; Bishop, 1985; O'Sullivan et al., 1996).

In stark contrast to such slow rates, Seidl et al. (1996) and Weisell and Seidl (1997) inferred a long-term average rate of 2 km m.y.^{-1} for escarpment retreat by assuming that the scarp retreated 200 km from the margin since rifting, 100 m.y. ago. This rate is 10 times higher than their bedrock erosion rates and they suggested that hillslope processes control escarpment retreat rates (Weissel and Seidl, 1998). On similar grounds, the head of the Bega Valley has retreated $\sim 500 \text{ m m.y.}^{-1}$ (50 km to the rift margin). Our maximum soil production rate of $53 \pm 3 \text{ m m.y.}^{-1}$ is only one-tenth of this value and sets the bound between weathering-limited and transport-limited landscapes: the escarpment face is a low, landslide-dominated cliff roughly 200 m higher than the study area. The large discrepancy in rates emphasizes the differences between lateral retreat and vertical lowering and shows that processes other than soil production and creep are setting escarpment retreat rates, such as landslides. It is critical that the differences between cliff retreat and soil production and transport rates be reconciled with field parameters for future landscape evolution models.

The widely used linear sediment transport law is shown here to inadequately capture the clear spatial variation of soil thickness across the landscape. Topographic curvature, a proxy for soil production, decreases linearly with increasing soil depth rather than exponentially, as predicted when setting equation 6 equal to equation 2. The expected exponential relationship is valid only for the divergent landscape (where $\partial H/\partial t = 0$), but the linear trend into the convergent hollow shows that soils are thinner than expected (Fig. 5). It is possible that overland flow contributes to this thinning, suggesting the need for thorough analyses of the morphologic signatures of combinations of the transport laws used in landscape evolution models. In conclusion, an independent test based on cosmogenic nuclide profiles from tors supports the steady-state local soil depth assumption. We also conclude that soil depths and lowering rates at the escarpment base have been constant over the exposure age of the underlying bedrock, although slow, morphologic change over longer time scales is implied by the spatial variation of lowering rates across the noses.

ACKNOWLEDGMENTS

We thank the landowners, Steve Bateman and his family for their assistance. D. Kelleher helped survey the site. This work was supported by National Science Foundation grant EAR-9527006, Institute of Geophysics and Planetary Physics—Lawrence Liver-

more National Laboratory (LLNL) grant GS96-05, and National Aeronautics and Space Administration Global Change and Switzer Environmental fellowships to Heimsath. Nuclide measurements were partially performed under the auspices of the U.S. Department of Energy by LLNL under contract W-7405-Eng-48. We thank Don DePaolo for laboratory space, and Darryl Granger and Greg Tucker for helpful reviews.

REFERENCES CITED

- Bishop, P., 1985, Southeast Australian late Mesozoic and Cenozoic denudation rates: A test for late Tertiary increases in continental denudation: *Geology*, v. 13, p. 479–482.
- Bureau of Meteorology, Australia, 1999, Climate averages for Bega, NSW, 1879–1996; Bombala, NSW, 1885–1996; and Nimmitabel, NSW, 1894–1996. Data printed from the Web: <http://www.bom.gov.au/climate/averages/>, December 1999.
- Butler, B.E., 1967, Soil periodicity in relation to landform development in southeastern Australia, in Jennings, J.N., and Mabbutt, J.A., eds., *Landform studies from Australia and New Guinea*: Cambridge, UK, Cambridge University Press, p. 231–255.
- Caine, N., and Jennings, J.N., 1968, Some blockstreams of the Toolong Range, Kosciusko State Park, New South Wales: *Royal Society of New South Wales Proceedings*, v. 101, p. 93–103.
- Costin, A.B., 1972, Carbon-14 dates from the Snowy Mountains area and their interpretation: *Quaternary Research*, v. 2, p. 579–590.
- Dunne, J., Elmore, D., and Muzikar, P., 1999, Scaling factors for the rates of production of cosmogenic nuclides for geometric shielding and attenuation at depth on sloped surfaces: *Geomorphology*, v. 27, p. 3–11.
- Galloway, R.W., 1965, Late Quaternary climates in Australia: *Journal of Geology*, v. 73, p. 603–618.
- Heimsath, A.M., Dietrich, W.E., Nishiizumi, K., and Finkel, R.C., 1997, The soil production function and landscape equilibrium: *Nature*, v. 388, p. 358–361.
- Heimsath, A.M., Dietrich, W.E., Nishiizumi, K., and Finkel, R.C., 1999, Cosmogenic nuclides, topography, and the spatial variation of soil depth: *Geomorphology*, v. 27, p. 151–172.
- Kooi, H., and Beaumont, C., 1994, Escarpment evolution on high-elevation rifted margins: Insights derived from a surface processes model that combines diffusion, advection, and reaction: *Journal of Geophysical Research*, v. 99, p. 12,191–12,209.
- Lal, D., 1991, Cosmic ray labeling of erosion surfaces: In situ nuclide production rates and erosion models: *Earth and Planetary Science Letters*, v. 104, p. 424–439.
- Lewis, P.C., and Glen, R.A., 1995, Bega-Mallacoota 1:250,000 geological sheet, SJ/55-4, SJ/55-8 (second edition): Sydney, Australia, Geological Survey of New South Wales.
- McKean, J.A., Dietrich, W.E., Finkel, R.C., Southon, J.R., and Caffee, M.W., 1993, Quantification of soil production and downslope creep rates from cosmogenic ^{10}Be accumulations on a hillslope profile: *Geology*, v. 21, p. 343–346.
- Nishiizumi, K., Winterer, E.L., Kohl, C.P., Klein, J., Middleton, R., Lal, D., and Arnold, J.R., 1989, Cosmic ray production rates of ^{10}Be and ^{26}Al in quartz from glacially polished rocks: *Journal of Geophysical Research*, v. 94, p. 17,907–17,915.
- Nott, J.F., 1992, Long-term drainage evolution in the Shoalhaven catchment, Southeast Highlands, Australia: *Earth Surface Processes and Landforms*, v. 17, p. 361–374.
- Ollier, C.D., 1982, The Great Escarpment of eastern Australia: Tectonic and geomorphic significance: *Geological Society of Australia Journal*, v. 29, p. 13–23.
- O'Sullivan, P.B., Foster, D.A., Kohn, B.P., and Gleadow, A.J.W., 1996, Multiple post-orogenic denudation events—An example from the Eastern Lachlan fold belt, Australia: *Geology*, v. 24, p. 563–566.
- Paton, T.R., Humphries, G.S., and Mitchell, P.B., 1995, *Soils: A new global view*: London, UCL Press Limited, 213 p.
- Prosser, I.P., Chappell, J., and Gillespie, R., 1994, Holocene valley aggradation and gully erosion in headwater catchments, south-eastern highlands of Australia: *Earth Surface Processes and Landforms*, v. 19, p. 465–480.
- Seidl, M.A., Weissel, J.K., and Pratson, L.F., 1996, The kinematics and pattern of escarpment retreat across the rifted continental margin of SE Australia: *Basin Research*, v. 8, p. 301–316.
- Tucker, G.E., and Slingerland, R.L., 1994, Erosional dynamics, flexural isostasy, and long-lived escarpments: A numerical modeling study: *Journal of Geophysical Research*, v. 99, p. 12,229–12,243.
- van der Beek, P., and Braun, J., 1999, Controls on post-mid-Cretaceous landscape evolution in the southeastern highlands of Australia: Insights from numerical surface process models: *Journal of Geophysical Research*, v. 104, p. 4945–4966.
- Weissel, J.K., and Seidl, M.A., 1997, Influence of rock strength properties on escarpment retreat across passive continental margins: *Geology*, v. 25, p. 631–634.
- Weissel, J.K., and Seidl, M.A., 1998, Inland propagation of erosional escarpments and river profile evolution across the southeast Australian passive continental margin, in Tinkler, K.J., and Wohl, E.E., eds., *Rivers over rock: Fluvial processes in bedrock channels*: American Geophysical Union Geophysical Monograph 107, p. 189–206.
- Wellman, P., 1987, Eastern Highlands of Australia; their uplift and erosion: *Bureau of Mineral Resources Journal of Australian Geology and Geophysics*, v. 10, p. 277–286.
- Wellman, P., and McDougall, I., 1974, Potassium-argon ages on the Cainozoic volcanic rocks of New South Wales: *Geological Society of Australia Journal*, v. 21, p. 247–272.
- Young, R.W., 1983, The tempo of geomorphological change: Evidence from southeastern Australia: *Journal of Geology*, v. 91, p. 221–230.

Manuscript received March 24, 2000

Revised manuscript received June 9, 2000

Manuscript accepted June 14, 2000